Vol. 23 • No. 8 • February 22 • 2011

D10488

www.advmat.de

ADVANCED MATERIALS

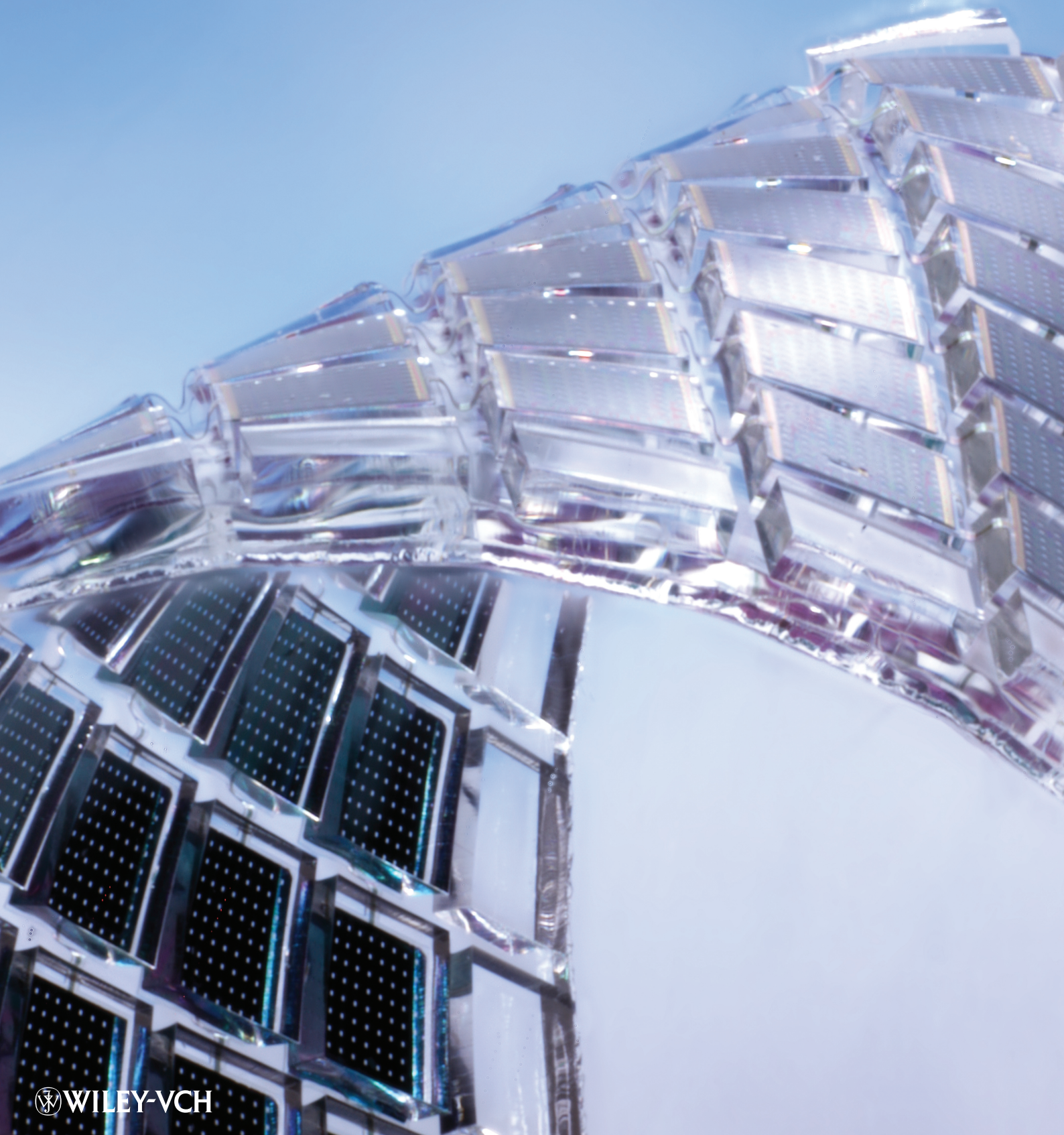

WILEY-VCH

Stretchable GaAs Photovoltaics with Designs That Enable High Areal Coverage

Jongho Lee, Jian Wu, Mingxing Shi, Jongseung Yoon, Sang-Il Park, Ming Li, Zhuangjian Liu, Yonggang Huang, and John A. Rogers**

Recent research in advanced materials and mechanics demonstrates the possibility for integrating inorganic semiconductors with soft, elastomeric substrates to yield systems with linear elastic mechanical responses to strains that significantly exceed those associated with fracture limits of the constituent materials (e.g. ~1% for many inorganics). This outcome can provide stretching to strain levels of tens of percent (in extreme cases, more than 100%), for diverse, reversible modes of deformation, including bending, twisting, stretching or compressing.[1–7] Interest in these outcomes is motivated by needs in flexible display,[8–10] curvilinear imaging devices,[11–13] structural health monitors[14] and, more recently, in bio-integrated systems[15–17] for advanced therapeutic or diagnostic functionality in clinical medicine. In these latter applications, considerations related to toxicity and biocompatibility of the materials are also critically important. Some of the most well developed strategies exploit configurations in which brittle, rigid materials accommodate in-plane strains through out-of-plane motions, via buckling or twisting modes.[18] Such ideas can be exploited in all parts of an integrated system, or only in interconnections between active devices. The latter design can accommodate the largest strains, but its efficacy decreases as the areal coverage of the devices increases.[12] As a result, important applications such as those in light capture (i.e., photovolatics) and detection (i.e., photodetectors), where high coverages are often desired, can be difficult to address. Here we report designs for stretchable systems that exploit elastomeric substrates with surface relief that confines strains at the locations of the interconnections, and away from the devices. The results enable areal coverages and levels of stretchability with relatively low interfacial stress between devices and substrates, compared to similar layouts with conventional, flat substrates. We describe, using a combination of theory and experiment, the essential mechanics, and then demonstrate the ideas in stretchable solar modules that use ultrathin, single junction GaAs solar cells.

A representative layout for a structured substrate designed for this purpose appears in **Figure 1**, in which the relief consists of isolated, raised regions (i.e. islands) separated by recessed features (i.e. trenches). The casting and curing processes of soft lithography[19] provide a convenient means to form such relief, with excellent dimensional control, in elastomers such as poly(dimethylsiloxane) (PDMS). The image of Figure 1a provides a cross sectional view for a representative case where square islands with edge lengths (l_{island}) of 800 μm are separated by trenches with widths (l_{trench}) and depths (h_{trench}) of 156 μm and 200 μm, respectively. The thickness of the underlying PDMS (i.e. base) is 200 μm. This type of structure is attractive for stretchable systems that incorporate non-stretchable active elements at the islands because it isolates strains from these regions. In particular, for this example, stretching the substrate (Figure 1b) to an overall strain of ~20% induces elongations (~123%) in the trenches that are much higher (>300 times) than those at the islands (~0.4%). The finite element method (FEM) quantitatively captures this basic mechanics, as shown in Fig 1b. In particular, for 20% overall strain, FEM yields a 124% increase in l_{trench} (i.e. 156 μm to 349 μm), which is very close to the value (~123%) obtained from experiment. FEM gives a very small change (0.3%) in l_{island}, similar to that (~0.4%) from experiments (see Supporting Information).

The resulting mechanics ensures that brittle inorganic devices mounted on the surfaces of the islands do not experience substantial mechanical stresses upon stretching or other mechanical deformations such as bending or twisting. This outcome obtains even for substrate layouts that consist primarily

Prof. J. A. Rogers
Department of Materials Science and Engineering
Chemistry, Mechanical Science and Engineering
Electrical and Computer Engineering
Beckman Institute for Advanced Science and Technology
and Frederick Seitz Materials, Research Laboratory
University of Illinois at Urbana-Champaign
Urbana, Illinois 61801, USA;
E-mail: jrogers@uiuc.edu
Prof. Y. Huang
Departments of Civil and Environmental Engineering
and Mechanical Engineering
Northwestern University
Evanston, Illinois 60208, USA
E-mail: y-huang@northwestern.edu
Dr. J. Lee, Dr. J. Yoon, Dr. S.-I. Park
Department of Materials Science and Engineering
Frederick Seitz Materials Research Laboratory
University of Illinois at Urbana-Champaign
Urbana, Illinois 61801, USA
Dr. J. Wu, M. Li
Department of Civil and Environmental Engineering
Northwestern University
Evanston, IL 60208, USA
Dr. M. Shi, Dr. Z. Liu
Institute of High Performance Computing
Singapore 138631, Singapore
M. Li
Department of Engineering Mechanics
Dalian University of Technology
Dalian, 116024, China

DOI: 10.1002/adma.201003961

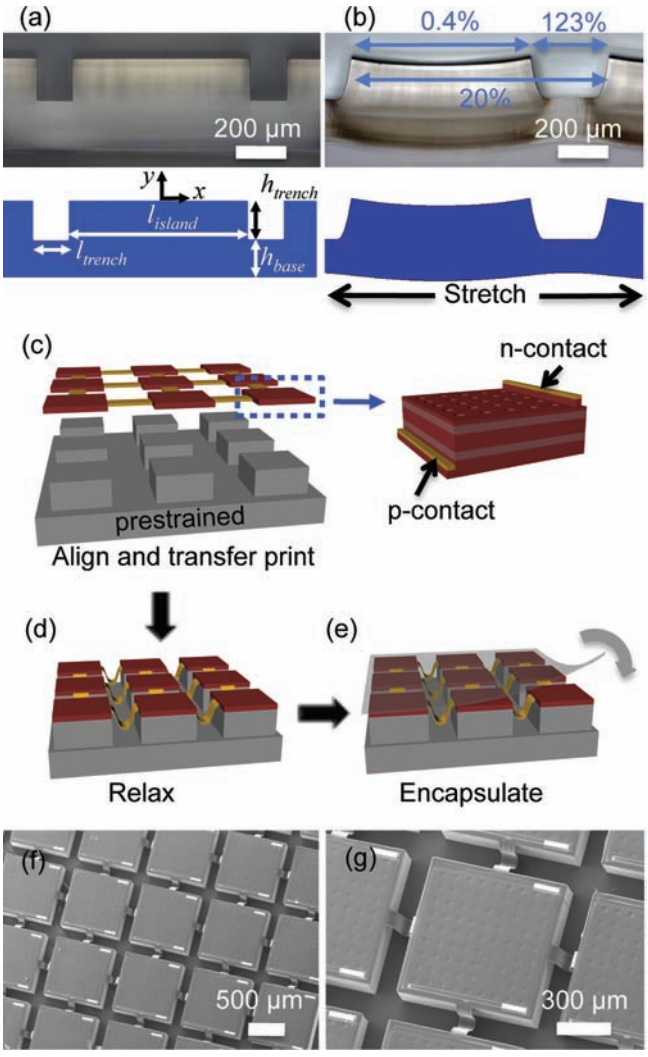

Figure 1. Optical microscopy images and finite element method (FEM) calculations of deformation of a slab of poly(dimethylsiloxane) (PDMS) and schematic illustrations of steps in the fabrication of stretchable GaAs photovoltaic modules with SEM images of a completed device. (a) Cross-sectional optical microscopy images (upper) and FEM (lower) of a slab of PDMS in relaxed (a) and stretched (b) states, with a square array of raised islands (each ~800 μm × 800 μm) separated by recessed trenches (widths ~156 μm, depths ~200 μm), designed as a platform for stretchable inorganic photovoltaics with high areal coverages. The latter image shows clearly that stretching (in this case, overall applied strain of 20%) induces dimensional changes at the top surfaces of the islands (~0.4%) that are much smaller than those at the trenches (~123%). This mechanics isolates devices located on the islands from applied strain. The FEM results show quantitative agreement with the experimental image in (b). (c) In the first step of the fabrication, an array of ultrathin GaAs microcells is bonded onto a prestrained, structured substrate of PDMS. Each microcell (size ~760 μm × 760 μm, thickness ~3.6 μm) has top (n) and bottom (p) Ohmic contacts that connect to thin electrical interconnect ribbons, in the overall geometry of an open mesh. (d) Releasing the pre-strain deforms the interconnects into arc-shaped bridges, usually in a vertical, upward orientation as illustrated here. Pressing on the entire array using a flat plate of glass causes these bridges to buckle downward, into the trench regions of the PDMS substrate. (e) In a final step, a thin (~50 μm), uniform layer of PDMS is bonded on top, as an encapsulant to protect the system from the environment. For purposes of imaging and electrical probing, the modules are left unencapsulated unless specifically noted. (f,g) SEM images of a completed module.

of islands, thereby making it possible to realize areal coverages of devices that are significantly higher than those achievable with conventional, flat substrate designs.[5–7,10] For photovoltaic modules that consist of interconnected arrays of an ultrathin, GaAs solar microcell technology,[20–22] the fabrication begins with vertical etching through active layers grown epitaxially on GaAs wafers, to define lateral dimensions of cells with sizes and spacings matched to the islands on the PDMS, in its biaxially prestrained state. Releasing these devices by etching a buried sacrificial layer of AlAs, and then performing further processing on a temporary substrate yields Ohmic contacts and thin ribbon-cable type interconnects between adjacent cells, as illustrated in the upper frames of Figure 1c. The inset on the right provides a schematic view of a single cell, with p and n contacts. The interconnects consist of films of gold (0.32 μm thick) coated on top and bottom with layers of an epoxy polymer (1.0 μm and 2.0 μm thicknesses on top and bottom, respectively). The GaAs microcells are 3.6 μm thick, and they include the same polymer coatings. See Supplemental Information for details. Another transfer printing step delivers the resulting mesh structure onto a prestrained structured PDMS substrate, as in the lower left frame of Figure 1c. Relaxing the strain (Figure 1d) induces compressive forces localized at the trenches, according to the mechanics of Figure 1b. The interconnects respond to this strain by buckling into arc-type shapes, most (>90%) with an upward orientation. Pressing down on the entire system with a flat, rigid plate causes the interconnects to buckle downward, into the trenches as shown in Figure 1d. The final step involves bonding a thin, uniform layer of PDMS on top, as illustrated in Figure 1e, to serve as an encapsulant, by exploiting interface covalent bonds that form between hydroxyl groups on the surface of the PDMS layer and a coating of SiO_2 evaporated on the devices, as described in the Supporting Information. The scanning electron microscopy (SEM) images of Figure 1f,g show a module, with the microcells and buckled interconnects clearly visible. Each microcell includes exposed regions at the p and n contacts to facilitate electrical measurements of individual devices.

Figure 2 shows these kinds of modules, in the relaxed state (Figure 2a), biaxially (Figure 2b) and uniaxially (Figure 2c) stretched, in a complex, twisting deformation (Figure 2d), laminated into sheets of fabric (Figure 2e) and paper (Figure 2f), and extremely bent (Figure 2g). The strains in the interconnect ($\varepsilon_{\text{interconnect}}$) and device islands ($\varepsilon_{\text{deviceisland}}$) for the as-fabricated state can be given analytically in terms of the overall strain ε

$$\varepsilon_{interconnect} = 4\pi y_{interconnect} \frac{[\varepsilon (l_{island} + l_{trench})]^{1/2}}{[\varepsilon l_{island} + (1+\varepsilon) l_{trench}]^{3/2}} \quad (1)$$

$$\varepsilon_{deviceisland} = 4\pi y_{deviceisland} \frac{[\varepsilon (l_{island} + l_{trench})]^{1/2}}{[\varepsilon l_{island} + (1+\varepsilon) l_{trench}]^{3/2}} \times \frac{(EI)_{intconnect}}{(EI)_{deviceisland}} \quad (2)$$

where $y_{interconnect}$ and $y_{deviceisland}$ are the distances to the neutral mechanical plane of the interconnect and device islands, respectively, and EI is the corresponding bending stiffness (see Supporting Information for details). For

ε = 20%, the maximum strains in gold (interconnect) and GaAs (device islands) are 0.94% and 0.22%, respectively. Consistent with expectation based on the mechanics of Figure 1b, uniaxial stretching by 20% induces 123% elongation in the trenches whose lengths lie perpendicular to the applied strain. Simultaneously, the trenches in the orthogonal direction narrow by 44%, due to the Poisson effect, which agrees well with the value (46%) from FEM, and can be estimated analytically (see Supporting Information for details)

$$contraction = \frac{v\varepsilon}{\frac{l_{trench}}{l_{island}+l_{trench}}\left(1+\frac{l_{trench}}{l_{island}+l_{trench}}\frac{h_{trench}}{h_{base}}\right)} \quad (3)$$

where v is the Poisson's ratio. This 44% contraction is equivalent to an overall strain of ε = –7.2%, as obtained from $\varepsilon\,(l_{island} + l_{trench}) / l_{trench} = -44\,\%$. The corresponding maximum strains in the gold interconnects and the GaAs are obtained from Equation (1) and (2) as 1.1% and 0.25%, respectively. The maximum strains in the polymer at the interconnects and device islands are 6.2% and 0.51%, respectively. Slight design modifications can reduce the strain in the interconnects. For example, by fixing the thicknesses of gold and polymer, but shifting the gold toward the neutral mechanical plane, the maximum strains in the gold and polymer can be reduced to 0.51% and 5.2%, respectively. Failures at large strain deformations are typically due to fracture of the metal layers in the interconnects. Further reductions can be achieved using interconnects with curved shapes.[5] Even with the relatively simple implementation here, the modules can be twisted into complex shapes (Figure 2d) without any damage to the devices or interconnects. These favorable mechanical properties also allow them to be integrated onto unusual substrates such as cloth (Figure 2e) and paper (Figure 2f). The module in Figure 2e is

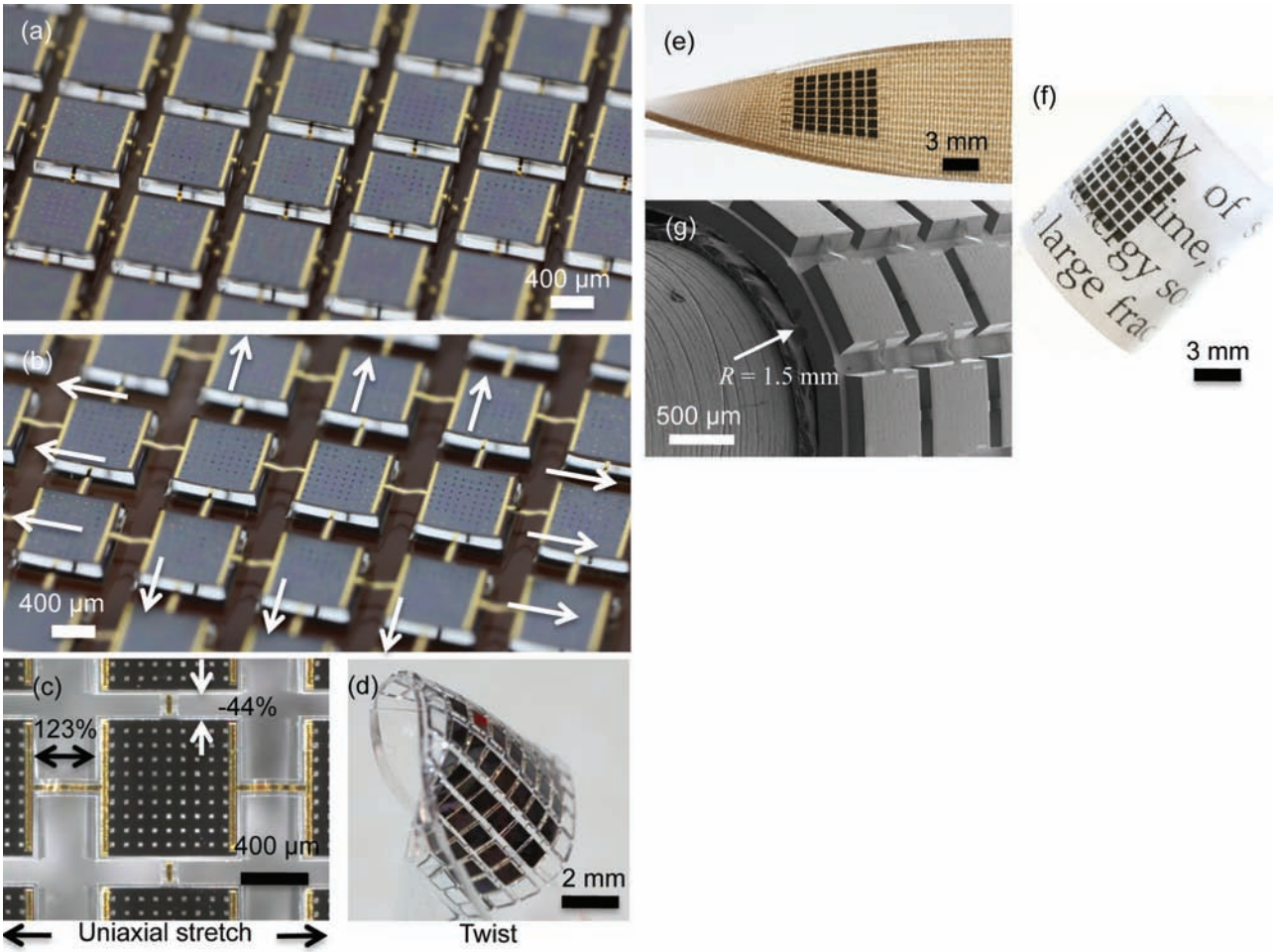

Figure 2. Optical microscope and SEM images of stretchable GaAs photovoltaic modules in various states of deformation and integrated onto different substrates. (a) Representative module, with a ~70% areal coverage of islands. (b) Similar module, in a state of 20% biaxial strain. Here, the regions of the trenches and islands stretch by ~123% and a negligible amount, respectively. This mechanics isolates the GaAs microcells from applied strain. (c) Module in a state of 20% uniaxial strain. Here, the widths of the trenches narrow (~44%) in the direction perpendicular to the stretching direction, due to the Poisson effect. In both directions, the dimensions of the islands change by a negligible amount. Quantitative analysis of the strain appears in the supplementary information. (d) Stretchable GaAs photovoltaic twisted into a complex shape, to illustrate the level of deformability. Similar module, laminated on a piece of cloth (e), twisted 90° over the length of 24 mm and paper (f), wrapped on a cylinder with a radius of 5.8 mm. (g) SEM image of the module wrapped on a cylinder with a radius of 1.5 mm.

twisted 90° over the length of 24 mm. The module in Figure 2f is wrapped on a cylinder with a radius of 5.8 mm.

A simple model predicts the minimum bending radius by assuming fracture upon further bending after fully straightening the interconnects. See Supporting Information for details. The calculated minimum bending radius is 1.4 mm. Experimental results in Figure 2g indicate that the module can wrap a cylinder with a radius of 1.5 mm with a little room to bend further as the interconnects are not fully straightened at the curvature. The island-trench design also maintains a flat geometry for the device islands, consistent with low strains at these locations, even at the extreme bending as shown in the SEM image in Figure 2(g). The trenches absorb the strain caused by bending the module. In this case, the calculated minimum bending radius of the module is 11.2 mm for the opposite direction, if we assume that failure occurs when the strain in the Au reaches 1%. With a higher prestrain (e.g. ~30%) and correspondingly longer interconnects, we can achieve, at the same as-fabricated areal coverage of ~70%, bending radii of 1.8 mm in both directions as described in Supporting Information.

Quantitative study of the mechanics by modeling and experiment defines the range of deformations that can be accommodated for different designs, including aspects such as the Poisson effects mentioned above and all others. Furthermore, the results allow comparison of the strategies reported here to systems based on conventional, flat PDMS substrates. The sizes of the devices, their spacings and other parameters are the same for both cases, as given in Figure 1, as are the total thicknesses (h_{base} + h_{trench} for the structured case). See **Figure 3a** and b. A key difference is that a biaxial prestrain of 20% gives a biaxial stretchability of 20% for the structured case; the flat substrate requires a larger prestrain to achieve the same stretchability. This behavior occurs because the prestrain stretches a flat substrate uniformly, but this strain does not fully relax in the regions of the devices due to their mechanical loading. In particular, analysis by FEM suggests that a biaxial prestrain of 30.0% is needed to achieve 20% stretchability in the flat case (see Supporting Information for details). Figure 3c–f show the distributions of shear and normal stresses at the interface between the microcells, for structured and flat substrates, respectively. The maximum shear and normal stresses for the structured substrate are about 8 and 7 times lower than those for the flat substrate, respectively. The structured geometry therefore offers a significant advantage against shear mode failures at the interface. Another difference between the structured and flat substrates, immediately observable in systems with high areal coverages, relates to overall bowing effects, similar to those previously explored by us in the context of uniform, rigid thin layers on soft substrates.[23] As illustrated in optical images and FEM results of Figure 3g,h, with the parameters and prestrains described previously, modules on flat substrates exhibit strong bowing, due to high interfacial stresses.

To demonstrate these devices and mechanics considerations in functioning modules, we evaluated the photovoltaic performance in relaxed (Figure 4a) and stretched (Figure 4b) states under using a solar simulator (Oriel, 91192) as shown in Figure 4c. The open circuit voltage and short circuit current of an individual microcell are 0.91 V and 88 μA respectively, as shown with the

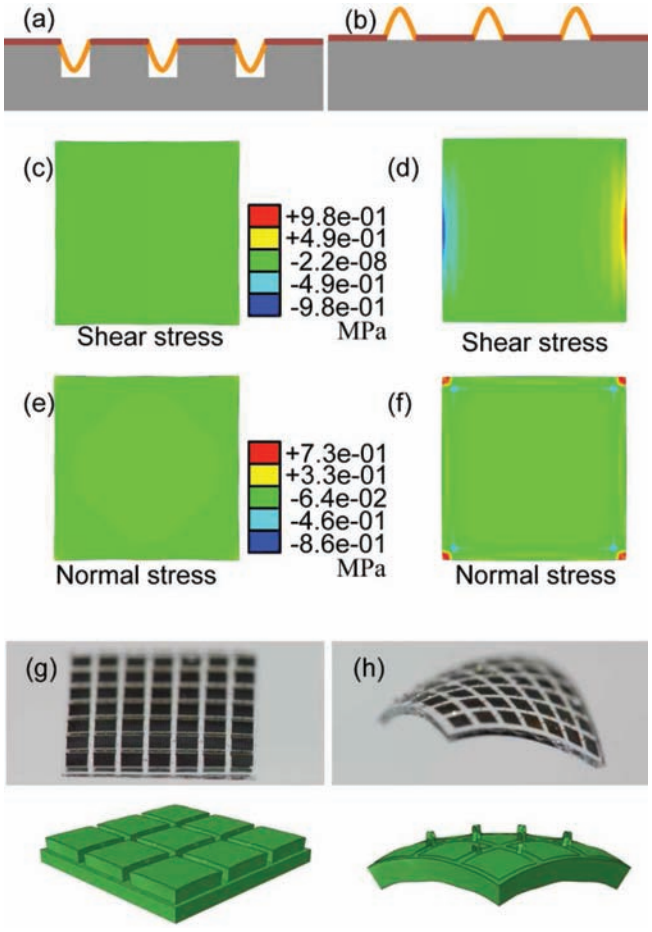

Figure 3. Finite element method (FEM) results for stretchable GaAs photovoltaic modules, consisting of interconnected arrays of devices in non-coplanar, mesh geometries, bonded to structured and flat elastomeric substrates. The islands (~800 μm × 800 μm) cover 70% of the structured substrate. The widths and depths of the trenches are 156 μm and 200 μm, respectively. The total thicknesses of the structured and flat substrate are both 400 μm. Schematic illustrations of the structured (a) and flat (b) cases. FEM results for the interfacial shear stresses between the devices and the structured (c) and flat (d) substrates. The maximum shear stress for structured substrate is eight times lower than this for the flat substrate. FEM result for the interfacial normal stresses between the devices and the structured (e) and flat (f) substrates. The maximum normal stress for the structured substrate is seven times lower than this for the flat substrate. (g) Bowing effects observed by experiments (upper) and FEM (lower) for devices on structured (g) and flat (h) substrates. For substrates with these thicknesses, bowing is pronounced in the flat case but not the structured case, due to comparatively high interfacial stresses between the devices and substrate for the former.

blue curve. Energy conversion efficiencies and fill factors are approximately 13% and 0.79, respectively, for each microcell. As expected, the open circuit voltage increases about seven times (~6.4 V) with seven microcells connected in series, in the relaxed state (Figure 4c, black curve). Biaxial stretching to 20% (red curve in Figure 4c) does not change these characteristics, to within experimental uncertainties. Furthermore, cycling tests involving repeated biaxial stretching to 20% followed by complete relaxation leave the performance unchanged. The efficiency (~12.5%)

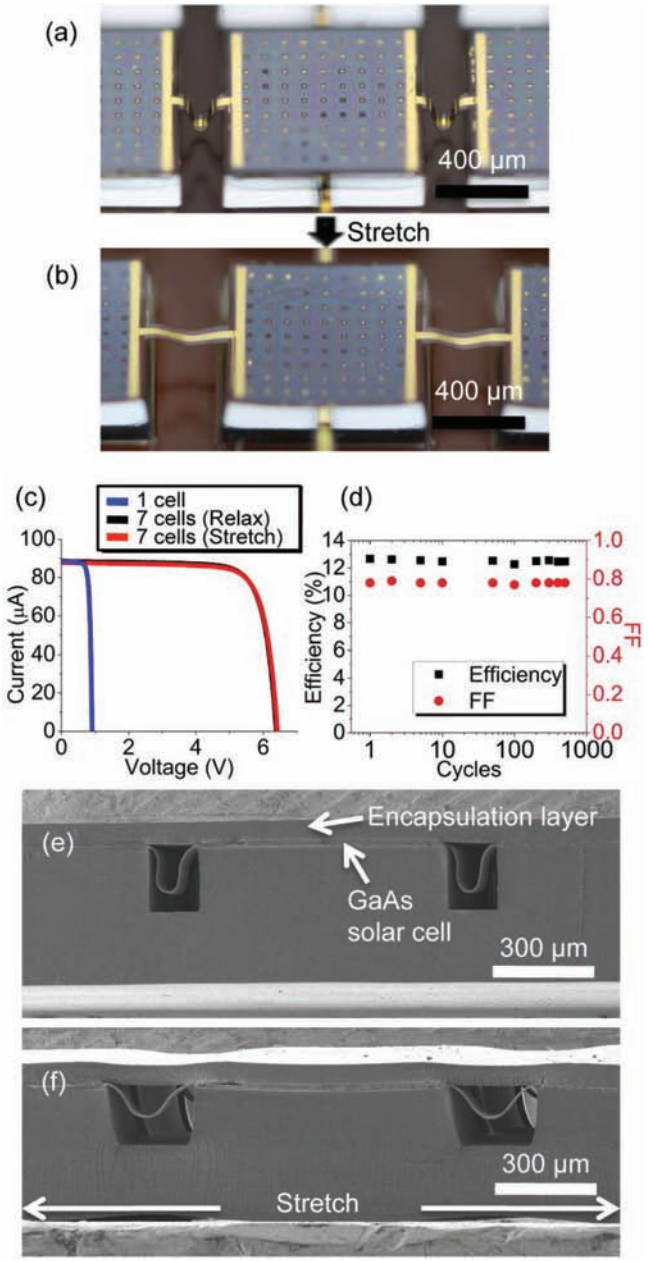

Figure 4. Optical microscope images and electrical characteristics of a representative stretchable GaAs photovoltaic module, and SEM images of encapsulated modules. Optical images of a part of the module in relaxed (a) and stretched (~20% biaxial) (b) states. (c) Current–voltage characteristics of a single microcell in the array (blue) and of seven microcells with series interconnections in relaxed (black) and stretched (red) states. (d) Experimental results of mechanical cycling tests. The data reveal no degradation in performance of the module with more than 500 cycles. (e) SEM cross-sectional image of an encapsulated module. The interconnects are clearly visible as arc-shaped structures in the sealed trenches of the substrate. (f) SEM image of a similar module, stretched uniaxially by 15%. The interconnects move freely to accommodate the applied strain.

and fill factor (FF, ~0.78) of the interconnected microcells are constant over more than 500 cycles. Related devices based on flat substrates offer similarly attractive fatigue response, but they do not allow, simultaneously, similar levels of coverage and stretchability without leading to high interfacial stresses that can cause adverse effects on the module such as the bowing effect.

Devices designed for realistic use require encapsulating layers to protect the devices and interconnects from the environment. Figure 4e and f presents results of systems encapsulated by thin (~50 μm) layers of PDMS. The procedures (Figure 1) maintain open cavities at the positions of the trenches, to retain the favorable, strain-isolating mechanics and to provide space for unrestricted motion of the interconnects (Figure 4e,f). Detailed FEM results are given in the Supporting Information.

The structural designs reported here are attractive for their simplicity, and their applicability not only to photovoltaics, but also to all other emerging areas of stretchable semiconductor device technologies. Although the structures studied here involve regular, square arrays of islands, other lattice geometries and even irregular configurations retain the same favorable mechanics. Finally, we note that additional refinements of the shapes and layouts for the interconnects as well as those of the islands can lead to further improvements. The additional flexibility in system design should be useful for many applications.

Experimental Section

Integrating the Interconnected Solar Microcells on the PDMS Substrate: A flat piece of PDMS was used to lift the interconnected GaAs solar microcells from their silicon substrate after dissolving the underlying layer of PMMA in acetone. Electron beam evaporation of Ti (5 nm) and SiO_2 (30 nm) on the back surfaces prepared the device for bonding with a prestrained, structured substrate of PDMS. Aligned bonding was accomplished using an assembly of translation and rotation stages, with an optical microscope. Annealing at 100 °C for 10 min enhanced the adhesion. Upon release of the prestrain, most of the interconnections between microcells buckled upward into non-coplanar, arc-shaped bridges. Pressing on the entire system with a flat glass plate caused these bridges to buckle downward into the recessed relief on the PDMS. See Supporting Information for further details on fabrication and measurement.

Supporting Information

Supporting Information is available from the Wiley Online Library or from the author.

Acknowledgements

We thank T. Banks for help with processing, using facilities at the Frederick Seitz Materials Research Laboratory. This material is based upon work supported by the Office of Naval Research. J. W. and Y. H. acknowledge the support from ISEN, Northwestern University.

Received: October 26, 2010
Published online: January 11, 2011

[1] D. S. Gray, J. Tien, C. S. Chen, *Adv. Mater.* **2004**, *16*, 393.
[2] S. P. Lacour, J. Jones, S. Wagner, T. Li, Z. G. Suo, *Proc. IEEE* **2005**, *93*, 1459.
[3] D. Brosteaux, F. Axisa, M. Gonzalez, J. Vanfleteren, *IEEE Electron Dev. Lett.* **2007**, *28*, 552.
[4] M. Gonzalez, F. Axisa, M. V. Bulcke, D. Brosteaux, B. Vandevelde, J. Vanfleteren, *Microelectron. Reliability* **2008**, *48*, 825.

[5] D. H. Kim, J. Z. Song, W. M. Choi, H. S. Kim, R. H. Kim, Z. J. Liu, Y. Y. Huang, K. C. Hwang, Y. W. Zhang, J. A. Rogers, *Proc. Natl. Acad. Sci. USA* **2008**, *105*, 18675.
[6] D. H. Kim, Y. S. Kim, J. Wu, Z. J. Liu, J. Z. Song, H. S. Kim, Y. G. Y. Huang, K. C. Hwang, J. A. Rogers, *Adv. Mater.* **2009**, *21*, 3703.
[7] D. H. Kim, Z. J. Liu, Y. S. Kim, J. Wu, J. Z. Song, H. S. Kim, Y. G. Huang, K. C. Hwang, Y. W. Zhang, J. A. Rogers, *Small* **2009**, *5*, 2841.
[8] T. Sekitani, Y. Noguchi, K. Hata, T. Fukushima, T. Aida, T. Someya, *Science* **2008**, *321*, 1468.
[9] T. Sekitani, H. Nakajima, H. Maeda, T. Fukushima, T. Aida, K. Hata, T. Someya, *Nat. Mater.* **2009**, *8*, 494.
[10] S. I. Park, Y. J. Xiong, R. H. Kim, P. Elvikis, M. Meitl, D. H. Kim, J. Wu, J. Yoon, C. J. Yu, Z. J. Liu, Y. G. Huang, K. Hwang, P. Ferreira, X. L. Li, K. Choquette, J. A. Rogers, *Science* **2009**, *325*, 977.
[11] H. C. Ko, M. P. Stoykovich, J. Z. Song, V. Malyarchuk, W. M. Choi, C. J. Yu, J. B. Geddes, J. L. Xiao, S. D. Wang, Y. G. Huang, J. A. Rogers, *Nature* **2008**, *454*, 748.
[12] G. Shin, I. Jung, V. Malyarchuk, J. Z. Song, S. D. Wang, H. C. Ko, Y. G. Huang, J. S. Ha, J. A. Rogers, *Small* **2010**, *6*, 851.
[13] I. Jung, G. Shin, V. Malyarchuk, J. S. Ha, J. A. Rogers, *Appl. Phys. Lett.* **2010**, *96*.
[14] R. Reuss, B. R. Chalamala, A. Moussessian, M. G. Kane, A. Kumar, D. C. Zhang, J. A. Rogers, M. Hatalis, D. Temple, G. Moddel, B. J. Eliasson, M. J. Estes, J. Kunze, E. S. Handy, E. S. Harmon, D. B. Salzman, J. M. Woodall, A. A. Alam, J. Y. Murthy, S. C. Jacobsen, M. Olivier, D. Markus, P. M. Campbell, E. Snow, *Proc. IEEE* **2005**, *93*, 1239.
[15] B. P. Timko, T. Cohen-Karni, G. H. Yu, Q. Qing, B. Z. Tian, C. M. Lieber, *Nano Lett.* **2009**, *9*, 914.
[16] J. Viventi, D. H. Kim, J. D. Moss, Y. S. Kim, J. A. Blanco, N. Annetta, A. Hicks, J. L. Xiao, Y. G. Huang, D. J. Callans, J. A. Rogers, B. Litt, *Science Translational Medicine* **2010**, 2.
[17] D. H. Kim, J. Viventi, J. J. Amsden, J. L. Xiao, L. Vigeland, Y. S. Kim, J. A. Blanco, B. Panilaitis, E. S. Frechette, D. Contreras, D. L. Kaplan, F. G. Omenetto, Y. G. Huang, K. C. Hwang, M. R. Zakin, B. Litt, J. A. Rogers, *Nat. Mater.* **2010**, *9*, 511.
[18] D. H. Kim, J. L. Xiao, J. Z. Song, Y. G. Huang, J. A. Rogers, *Adv. Mater.* **2010**, *22*, 2108.
[19] Y. N. Xia, G. M. Whitesides, *Ann. Rev. Mater. Sci.* **1998**, *28*, 153.
[20] M. Konagai, M. Sugimoto, K. Takahashi, *J. Crystal Growth* **1978**, *45*, 277.
[21] J. J. Schermer, P. Mulder, G. J. Bauhuis, P. K. Larsen, G. Oomen, E. Bongers, *Progr. Photovoltaics* **2005**, *13*, 587.
[22] J. Yoon, S. Jo, I. S. Chun, I. Jung, H. S. Kim, M. Meitl, E. Menard, X. L. Li, J. J. Coleman, U. Paik, J. A. Rogers, *Nature* **2010**, *465*, 329.
[23] S. D. Wang, J. Z. Song, D. H. Kim, Y. G. Huang, J. A. Rogers, *Appl. Phys. Lett.* **2008**, 93.

ADVANCED MATERIALS

Supporting Information

for *Adv. Mater.*, DOI: 10.1002/adma. 201003961

Stretchable GaAs Photovoltaics with Designs That Enable High Areal Coverage

Jongho Lee, Jian Wu, Mingxing Shi, Jongseung Yoon, Sang-Il Park, Ming Li, Zhuangjian Liu, Yonggang Huang ,* and John A. Rogers *

Submitted to ADVANCED MATERIALS

Supporting Information for

Stretchable GaAs Photovoltaics With Designs That Enable High Areal Coverage

By *Jongho Lee, Jian Wu, Mingxing Shi, Jongseung Yoon, Sang-Il Park, Ming Li, Zhuangjian Liu, Yonggang Huang* and John A. Rogers**

[*] Prof. John A. Rogers Corresponding-Author

Department of Materials Science and Engineering, Chemistry, Mechanical Science and Engineering, Electrical and Computer Engineering

Beckman Institute for Advanced Science and Technology, and Frederick Seitz Materials Research Laboratory

University of Illinois at Urbana-Champaign

Urbana, Illinois 61801 (USA)

E-mail: jrogers@uiuc.edu

[*] Prof. Yonggang Huang Co-corresponding-Author

Departments of Civil and Environmental Engineering, and Mechanical Engineering

Northwestern University

Evanston, Illinois 60208 (USA)

E-mail: y-huang@northwestern.edu

Dr. Jongho Lee, Dr. Jongseung Yoon, Dr. Sang-Il Park

Department of Materials Science and Engineering

Frederick Seitz Materials Research Laboratory

University of Illinois at Urbana-Champaign

Urbana, Illinois 61801 (USA)

Dr. Jian Wu, Mr. Ming Li

Department of Civil and Environmental Engineering

Northwestern University

Evanston, IL 60208 (USA)

Dr. Mingxing Shi, Dr. Zhuangjian Liu

Institute of High Performance Computing

Singapore 138631

Keywords: stretchable electronics, photovoltaics, gallium arsenide

Deformation of structured substrate

As shown in Fig. 1, a structured substrate consists of isolated, raised square islands with edge lengths (l_{island}) of 800 μm separated by trenches with widths (l_{trench}) and depths (h_{trench}) of 156 μm and 200 μm, respectively. Finite element method (FEM) is used to study the deformation of structured substrate under uniaxial stretching. A unit cell, consisting of a single island and the base (below the trench), is subject to a uniform horizontal displacement on its side. The structured substrate (Young's modulus 1.8 MPa and Poisson's ratio 0.48) is modeled by the plane strain element CPE4R in the ABAQUS finite element program. Finite element mesh has been refined to ensure the convergence of the results. Figure S1b and c show the FEM results for the strain along x (ε_{xx}) as a function of position x, for various values of the thickness of the bases (h_{base}) and the depth of the trenches (h_{trench}) with other dimensions given above. The thickness of the base (h_{base}) is chosen to be as thin as possible, but sufficiently thick to allow casting/curing and handling without fracture. The depth of the trenches is close to the optimum value ($h_{trench} \sim 230$ μm) that minimizes the strains at the top surfaces of the islands.

Strains in interconnect and GaAs microcell

The mesh structure in Fig. 1 consists of the interconnects and the GaAs microcells. It is transfer printed onto a prestrained structured substrate. The interconnects consist of gold film (thickness 0.32 μm, Young's modulus 78 GPa and Poisson's ratio 0.44) coated on top and

bottom with layers of an epoxy polymer (1.0 μm and 2.0 μm thicknesses on top and bottom, respectively). The GaAs microcells (thickness 3.6 μm, Young's modulus 77.5 GPa and Poisson's ratio 0.312) are coated on top and bottom with layers of epoxy polymer (2.0 μm and 1.0 μm thicknesses on top and bottom, respectively). The Young's modulus and Poisson's ratio of epoxy polymer are 4.4 GPa and 0.44, respectively. The interconnects is modeled as a composite beam with effective bending stiffness

$$\left(EI\right)_{intconnect} = \sum_{i=1}^{3} \bar{E}_i h_i \left[\left(\sum_{j=1}^{i} h_j \right)^2 - \left(\sum_{j=1}^{i} h_j \right) h_i + \frac{h_i^2}{3} \right] - \frac{\left[\sum_{i=1}^{3} \bar{E}_i h_i \left(\sum_{j=1}^{i} h_j - \frac{h_i}{2} \right) \right]^2}{\sum_{i=1}^{3} \bar{E}_i h_i}$$

, where the summation is for the 3 layers of gold film and two coating epoxy polymer, h_i is the thickness of the i^{th} layer (from the top), and $\bar{E}_i = E_i / \left(1 - v_i^2\right)$ is related to the Young's modulus E_i and Poisson's ratio v_i of the i^{th} layer. The distance between the neutral mechanical plane and the top surface in each cross section is given by $\sum_{i=1}^{3} \bar{E}_i h_i \left(\sum_{j=1}^{i} h_j - \frac{h_i}{2} \right) \Big/ \sum_{i=1}^{3} \bar{E}_i h_i$. The strain in interconnects is given by $y\kappa$, where κ is the bending curvature, and y is the distance from the neutral mechanical plane.

A straight bridge buckles upon the release of prestrain, ε, in the structured substrate. The maximum curvature of interconnects is given by [1]

$$\kappa = 4\pi \frac{\left[\varepsilon \left(l_{island} + l_{trench} \right) \right]^{1/2}}{\left[\varepsilon l_{island} + \left(1 + \varepsilon\right) l_{trench} \right]^{3/2}} . \qquad \text{(S1)}$$

The microcells are also modeled as a composite beam, with the effective bending stiffness similar to that for the interconnects. The maximum strain in GaAs microcell can be obtained analytically [1], as given in Eq. (2).

Uniaxial stretching

Force equilibrium along the stretching direction requires $\varepsilon_{island}\left(h_{base}+h_{trench}\right)=\varepsilon_{base}h_{base}$, where ε_{island} and ε_{base} are the average tensile strains along the stretching direction in the island and in the base (below the trench), respectively. For an applied stretching strain ε, the total elongation $\varepsilon\left(l_{island}+l_{trench}\right)$ of a unit cell (one island plus one trench) is the sum of the elongations of the island, $\varepsilon_{island}l_{island}$, and base (below the trench), $\varepsilon_{base}l_{trench}$. This gives the strain in the island as $\varepsilon_{island}=\dfrac{\varepsilon}{1+\dfrac{l_{trench}}{l_{island}+l_{trench}}\dfrac{h_{trench}}{h_{base}}}$.

The islands and base (below the trench) contract in the lateral direction due to the Poisson's effect. The compressive strain in the island is $\dfrac{-\nu\varepsilon}{1+\dfrac{l_{trench}}{l_{island}+l_{trench}}\dfrac{h_{trench}}{h_{base}}}$. The compressive strain in the base (below the trench) is approximately the same because the base (below the trench) is much narrower than the islands such that its deformation is fully constrained by the islands. The total contraction of the unit cell (one island plus one trench) is $\dfrac{-\nu\varepsilon}{1+\dfrac{l_{trench}}{l_{island}+l_{trench}}\dfrac{h_{trench}}{h_{base}}}\left(l_{island}+l_{trench}\right)$. Since the deformation of the top surface of the islands is negligible as compared to that of the base, this contraction is absorbed by the reduction of trench width. This gives the contraction in Eq. (3).

FEM results for the deformation of devices

FEM is used to study the deformations of structured and flat substrates together with devices on the islands. Twenty five (5*5) islands on the base are first stretched equi-biaxially in the simulation. The devices are then adhered to the top of stretched island. The entire structure is then relaxed. The dimensions and material parameters are the same as described above. The substrates are modeled by the hexahedron element C3D8R in the ABAQUS finite element program, while the interconnects and GaAs microcells are modeled by the composite shell element S4R.

The encapsulation (epoxy polymer) layer is added to the relaxed structure, which is then subject to equi-biaxial stretching. The encapsulation layer is also modeled by hexahedron element C3D8R.

FEM results for encapsulation layers

FEM results indicate that increasing the thickness (h_{encap}) of the encapsulation layer reduces the maximum strain of the microcells under biaxial stretching by 20% as shown in Figure S4b; bending of the top surfaces of the islands is the primary cause of this strain. Thick encapsulation layers reduce the degree of this bending. On the other hand, increasing h_{encap} increases the interfacial shear stress between the device and the flat encapsulation layer as in Figure S4c. Simultaneously increasing the thickness and lowering the modulus of this layer can relax these competing effects, because the bending stiffness, EI, is linear in modulus but cubic in thickness. The FEM results in Figure S4c and d indicate that increasing h_{encap} decreases the strain (ε_{xx}) in the devices and the interfacial stress (τ_{yx}) at the same time, provided that the modulus is reduced to maintain a constant bending stiffness.

Bending of the module

The module was bent outward to wrap on a cylinder of radius R. The neutral mechanical plane is the middle plane of the base, which gives the bend radius $R+\frac{h_{\text{base}}}{2}$. The minimal bend radius corresponds to the limit when the buckled interconnects are stretched to flat, and the stretchability of the module ε is reached. From the beam theory ε equals the product of curvature $\left(R+\frac{h_{\text{base}}}{2}\right)^{-1}$ and the distance to the neutral mechanical plane, $h_{\text{trench}}+\frac{h_{\text{base}}}{2}$. This value relates the minimal radius R of the cylinder to the stretchablility ε as $R=\frac{(1-\varepsilon)h_{\text{base}}}{2\varepsilon}+\frac{h_{\text{trench}}}{\varepsilon}$. For $\varepsilon=20\%$, $h_{\text{base}}=200\ \mu\text{m}$ and $h_{\text{trench}}=200\ \mu\text{m}$, the minimal radius of the cylinder is 1.4 mm.

For the module wrapped inward (in the opposite direction) around the cylinder, the interconnects are further compressed. The bend radius $R+h_{\text{trench}}+\frac{h_{\text{base}}}{2}$ reaches the minimum when the strain in the gold layer of buckled interconnects reaches its failure strain, $\varepsilon_{\text{fail}}$. This gives the minimal radius R of the cylinder as $R=\frac{1-\bar{\varepsilon}}{\bar{\varepsilon}}\left(h_{\text{trench}}+\frac{h_{\text{base}}}{2}\right)$, where

$\bar{\varepsilon}=\frac{\varepsilon_{\text{fail}}^2\left[\varepsilon l_{\text{island}}+(1+\varepsilon)l_{\text{trench}}\right]^3}{16\pi^2 y_{\text{interconnect}}^2\left(l_{\text{island}}+l_{\text{trench}}\right)}-\varepsilon$. For $\varepsilon=29\%$, $\varepsilon_{\text{fail}}=1\%$, $l_{\text{island}}=800\ \mu\text{m}$, $l_{\text{trench}}=156\ \mu\text{m}$, $y_{\text{interconnect}}=0.35\ \mu\text{m}$, $h_{\text{base}}=200\ \mu\text{m}$ and $h_{\text{trench}}=200\ \mu\text{m}$, the minimal radius of the cylinder is 1.8 mm for both inward and outward bending.

Experimental

Fabricating GaAs Solar Microcells: We formed GaAs solar microcells using procedures described previously,[20] starting with a specialized epitaxial stack deposited on a GaAs wafer, with a sacrificial layer of AlAs on its surface. Patterned wet etching exposed p and n contact

regions, as well as holes through the thicknesses of the microcells to facilitate their release via elimination of the AlAs layer with hydrofluoric acid. Patterned structures of photoresist (PR, AZ5214) held the cells in their lithographically defined locations, thereby preparing them for transfer printing.

Transfer Printing, Establishing Ohmic Contacts and Forming Anti Reflective Coatings: The microcells were lifted onto the surface of a PDMS stamp (Sylgard 184, Dow Corning) after anchoring with photo resist (PR, AZ5214). Transfer printing delivered them to a layer of epoxy (1 μm SU8, Microchem) spin cast on a film of poly(methylmethacrylate) (1 μm, PMMA) on a glass slide. Sequential electron beam deposition of Pd (5 nm), Ge (35 nm) and Au (80 nm) on the n-contact regions of the microcells formed Ohmic contacts upon annealing at 175°C in an N_2 environment for 1 hour. Other contact metals, Pt (10 nm), Ti (40 nm), Pt (10 nm) and Au (80 nm), deposited in similar fashion but without annealing yielded Ohmic p-contacts. Silicon Nitride (Si_3N_4, 70 nm), deposited by plasma enhanced chemical vapor deposition (PECVD, SLR series, Plasma-Therm) formed anti-reflective coatings (ARCs).

Defining Electrical Interconnects and Encapsulating the Microcells: A bilayer of Ti (20 nm) and Au (300 nm) patterned on a film of SU8 (1 μm) with openings in the n- and p-contact regions formed series interconnects between the microcells. Spin casting yielded another layer of SU8 (1 μm) as an encapsulant, photodefined to provide openings in regions at the n- and p-contact metals of all the cells for electrical probing. Photolithography defined masking layers fort the island and bridge regions, in SiO_2 (150 nm) deposited by PECVD. Reactive ion etching (RIE, 790 series, Plasma-Therm; 50 m Torr, 150 W, CF_4 ~ 40 SCCM, O_2 ~ 1.2 SCCM, 8 min) of the exposed SiO_2 formed a hard mask on the SU8. Separate reactive ion etching (CS-1701, March, 150 mTorr, 150 W, O_2 ~ 20 SCCM, 50 min) of the SU8 through the hard mask defined the mesh structure.

Forming the Structured PDMS Substrate: Casting and curing methods of soft lithography [19] were used to form the structured PDMS substrates. The masters for this process consisted of thick layers of SU8 (~200 μm) photopatterned on silicon wafers. A mixture of silicone elastomer base and curing agent (10:1, Sylgard 184, Dow corning) was poured on the master and then cured at 70°C for 1 hour. Peeling back the cured PDMS completed the fabrication.

Encapsulating the Modules with Thin PDMS: Spin casting and thermal curing PDMS formulations identical to those for the substrates formed thin films for encapsulation. The bonding process involved deposition of Ti (5 nm) and SiO_2 (roughly 10-50 nm) onto the surfaces of the modules, and then contact with the PDMS layer while heating at 100 C for 10 min.

Measuring the Electrical and Mechanical Characteristics: The performance of the modules was measured under a 1000 W full spectrum solar simulator (Oriel, 91192) using a d.c. sourcemeter (model 2400, Keithley). The current-voltage (I-V) data from the interconnected cells were collected when the solar module was stretched and released.

[1] J. Song, Y. Huang, J. Xiao, S. Wang, K. C. Hwang, H. C. Ko, D.-H. Kim, M. P. Stoykovich, and J. A. Rogers, Journal of Applied Physics **2009**, 105, 123516.

Figure S1. (a) Schematic illustration of structured substrate. The square islands with edge lengths of 800 μm are separated by trenches with widths and depths of 156 μm and 200 μm, respectively. (b) FEM results for the strain along x (e_{xx}) as a function of position x, for various values of the depths of the trenches (h_{trench}) with 200 mm-thick base and other dimensions given above. The results indicate that, for this example, $h_{trench} \sim 230$ mm minimizes the strain at the top surfaces of the islands. (c) FEM results for the strain along x (ε_{xx}) as a function of position x, for various values of the thickness of the base (h_{base}). The results indicate that the strain at the top surface increases with the base thickness.

Figure S2. Schematic illustration of the dimensions of interconnects, microcells and structured substrate.

Figure S3. (a) Schematic illustration of structured case and results of analytical model. (b) The maximum strains in the gold film and (c) GaAs microcell as the function of length of stretched trench, $\lambda_{\text{interconnector}}$.

Figure S4. (a) Schematic illustration of encapsulated structured case and results from the finite element method (FEM). (b) Maximum tensile strain in the microcells obtained by FEM as a function of position along their width (x) for encapsulating layers with different thicknesses for the case of biaxial stretching to 20%. These strains arise primarily from slight bending induced at the top surfaces of the islands on the structured PDMS substrate. As the thickness of the encapsulation layer increases, the bending decreases, thereby reducing the strain. (c) Interfacial shear stress obtained by FEM as a function of position along x for various thicknesses of the encapsulation layer. Shear stress increases with thick encapsulating layer. (d) Maximum tensile strain in the microcells obtained by FEM as a function of position along their width (x) for encapsulating layers with different thicknesses and moduli, for the

case of biaxial stretching to 20%. These strains arise primarily from slight bending induced at the top surfaces of the islands on the structured PDMS substrate. As the thickness of the encapsulation layer increases while keeping the bending stiffness (*EI*) the same by reducing its modulus, the bending decreases, thereby reducing the strain. (e) Interfacial shear stress obtained by FEM as a function of position along *x* for various thicknesses of the encapsulation layer. Increasing the thickness while reducing the modulus decreases the stress.

Figure S5. (a) Schematic illustration of the solar module with the structural parameters indicated and (b) the module wrapped on a cylinder.

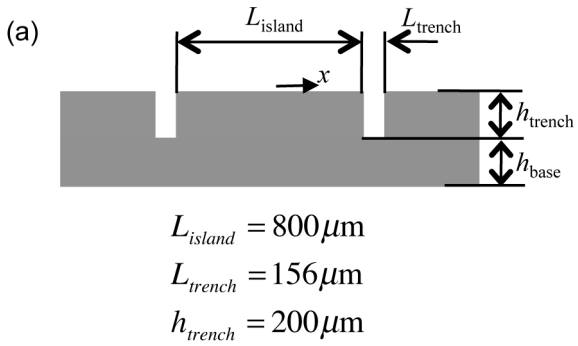

$$L_{island} = 800\mu\text{m}$$
$$L_{trench} = 156\mu\text{m}$$
$$h_{trench} = 200\mu\text{m}$$

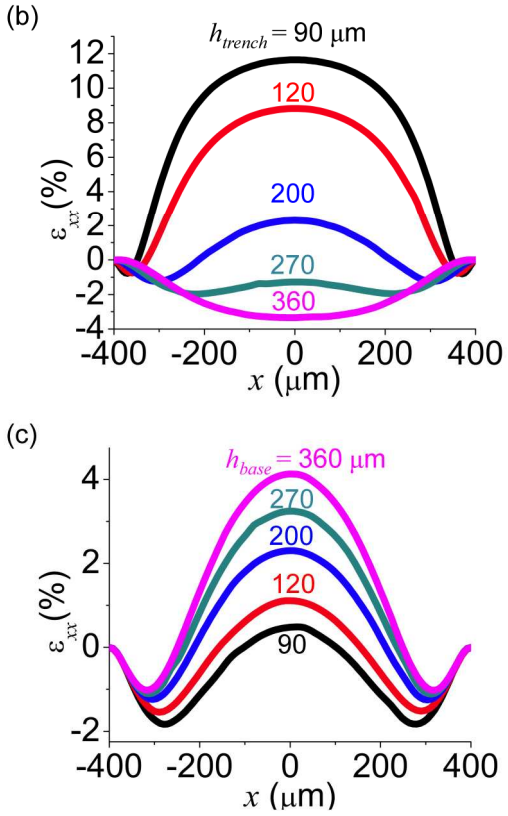

Figure S1

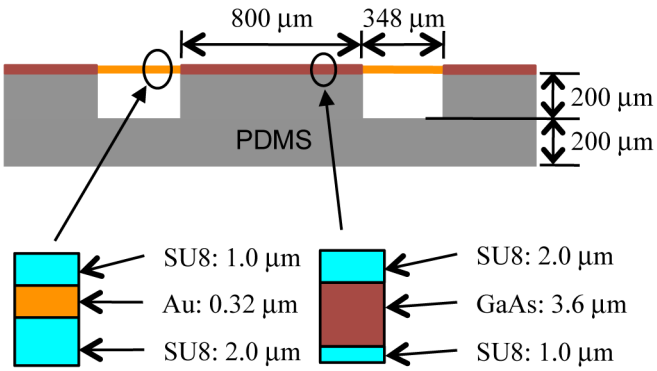

20% prestrain

Elastic modulus:

E_{au} = 78 GPa,
E_{SU8} = 4.4 Gpa,
E_{GaAs} = 77.5 GPa

Poisson ratio:

ν_{Au} =0.44,
ν_{SU8} =0.44,
ν_{GaAs} =0.312

Figure S2

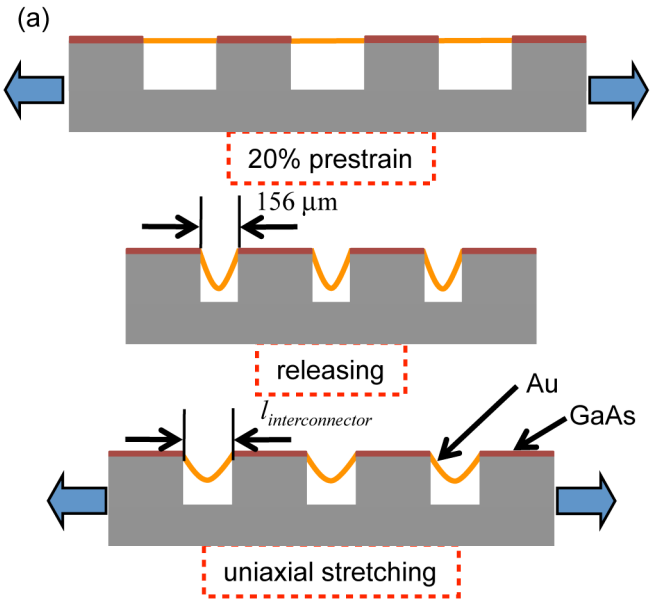

$$\lambda_{interconnector} = \frac{l_{interconnector} - 156}{156}$$

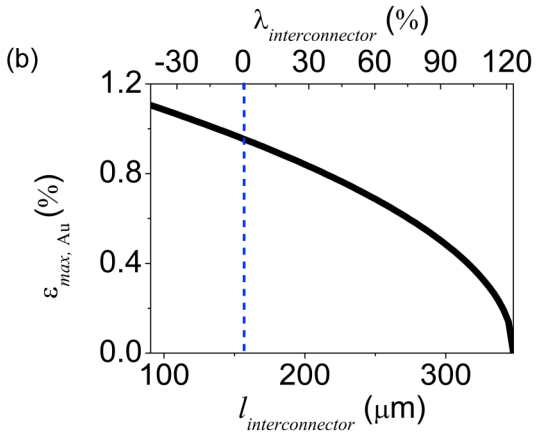

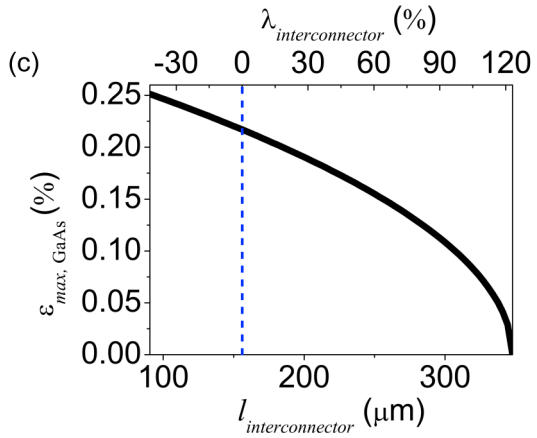

Figure S3

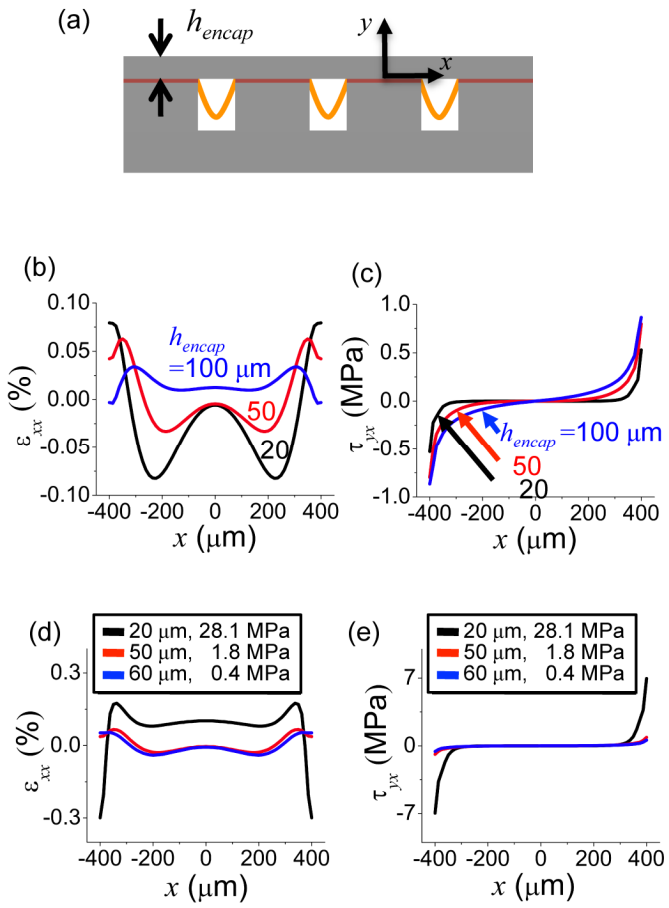
(a)
h_{encap}
y
x
(b)
h_{encap} =100 μm
50
20
ε_{xx} (%)
x (μm)
(c)
h_{encap} =100 μm
50
20
τ_{yx} (MPa)
x (μm)
(d)
20 μm, 28.1 MPa
50 μm, 1.8 MPa
60 μm, 0.4 MPa
ε_{xx} (%)
x (μm)
(e)
20 μm, 28.1 MPa
50 μm, 1.8 MPa
60 μm, 0.4 MPa
τ_{yx} (MPa)
x (μm)

Figure S4

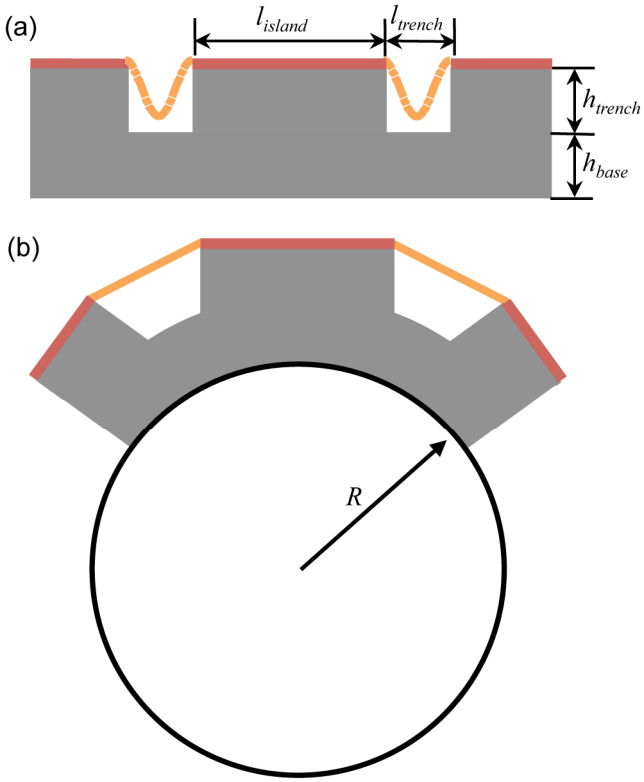

Figure S5